Italian Association of Aeronautics and Astronautics
XXVI International Congress
31st August – 3rd September 2021
On-line event hosted by the Tuscany AIDAA Section in Pisa

POD AND SPOD ANALYSIS OF VERTICAL LIQUID SHEET

A. Colanera[1*], M. Chiatto[1], L. de Luca[1]

[1]Department of Industrial Engineering, Università degli Studi di Napoli "Federico II", p.le Tecchio 80, 80125, Naples, Italy

*antonio.colanera@unina.it

ABSTRACT

Modal analysis of thin liquid sheet driven by a harmonic forcing in the lateral velocity component at the inlet section is performed. Proper orthogonal decomposition (POD) and spectral POD (SPOD) techniques have been applied on two-dimensional two-phase numerical simulations data, obtained with the VOF approach, to characterize the main spatial and temporal structures. The investigation is carried out varying the Weber number and the Reynolds number. In supercritical regime (Weber number, $We > 1$) both POD and SPOD techniques yield only leading sinuous modes, featuring a traveling perturbation. Spectral analysis confirms the occurrence of a discontinuity in frequency response between the supercritical and subcritical regimes. In subcritical regime ($We < 1$) the excitation of a combined sinuous-varicose motion is detected when the system is driven at resonance frequency for relatively high Reynolds numbers.

Keywords: liquid sheet; modal analysis; POD; SPOD

1 INTRODUCTION AND METHODOLOGY

Liquid sheet flows are an industrial and technologically interesting class of flows, whose governing equations presents challenging issues being object of investigation since the 50s of the last century. These flows are employed in a great variety of technological sectors, such as the paper making and the curtain coating processes.

The present paper aims at performing a modal decomposition analysis of viscous thin liquid sheets to extract the spatially and dynamically most relevant structures of this flow. For this purpose, two different modal techniques have been used, namely the proper orthogonal decomposition (POD), see Berkooz *et al.* [1], and the spectral proper orthogonal decomposition (SPOD), see Towne *et al.* [2] and Schmidt *et al.* [3]. In particular, the POD is a modal decomposition technique that provides the minimal number of modes to capture as much energy as possible. The SPOD technique allows one to characterize the spatial and temporal evolution of coherent structures through the decomposition of the flow in various modes, each one with an own frequency. Both techniques have been here applied to numerical data of two-dimensional flow fields simulated by means of the two-phase code BASILISK, see Popinet [4].

1.1 Numerical simulation layout

Numerical data of thin liquid sheet flows have been obtained through the single-phase formulation and the Volume-of-Fluid (VOF) approach, as shown in Scardovelli and Zaleski [5]. For the governing equations and further details on this method the reader can refer to Della Pia *et al.* [6]. The configuration consists in a forced liquid sheet, with a parabolic u velocity profile at the inlet of width H, which is perturbed by a sinusoidal forcing in the lateral velocity component v of amplitude $\hat{A}U$, where U is the mean velocity at the inlet and $\hat{A}$ a given dimensionless parameter. Simulations have been carried out in both supercritical, $We = \rho_l U^2 H/(2\sigma) > 1$, and subcritical, $We < 1$, regimes, ρ_l is the density of the liquid phase while σ is the surface tension. Main parameters of the analyzed cases are reported in Table 1.

	a	*b*	*c*	*d*	*e*	*f*	*g*	*h*	*i*
We	2.5	0.75	0.75	0.75	0.75	0.70	0.80	0.85	0.90
$Re = \rho UL/\mu_l$	400	20	400	1200	1600	1600	1600	1600	1600
$St_a = f_a H/U$	0.076	0.076	0.076	0.076	0.076	0.076	0.076	0.076	0.076

Table 1: Main parameters of analyzed cases

A sketch of the analyzed region and main geometric parameters are reported in Figure 1 panel (a). All simulations have been carried out at Froude number $Fr = U^2/(gL) = 0.33$, with a density ratio $r_\rho = \rho_g/\rho_l = 0.01$ (ρ_g being the ambient phase density) and with a sampling rate $f_s = 200\ Hz$. Panel (c) of Figure 1 reports a sample snapshot of the volume of fraction *C*.

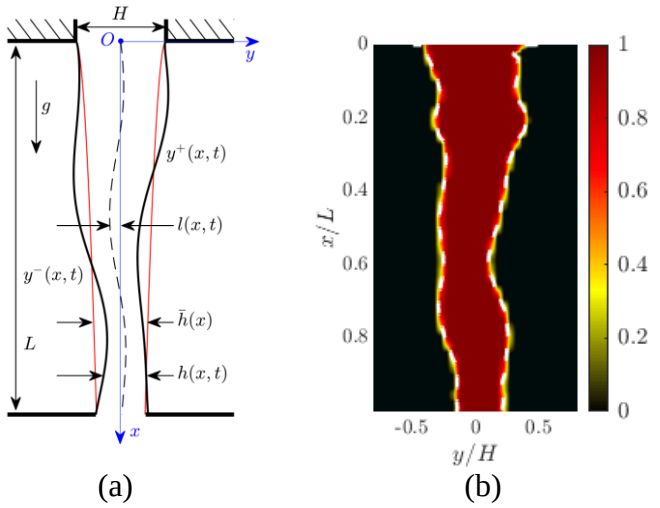

Figure 1: Typical numerical arrangement and sample output of the supercritical case (a) of Table 1. The white dashed lines represent the interface between phases.

1.2 POD technique

Proper Orthogonal Decomposition, POD, is a modal technique that extracts an optimal set of eigenfunctions forming a spatial orthogonal basis, see Berkooz *et al.* [1]. POD modes φ_k are the eigenvectors of the covariance matrix $\mathbf{QQ}^*$, where $\mathbf{Q}$ is the snapshot matrix containing in each column the state vector $\mathbf{q}$ for each timestep. In this application state vector $\mathbf{q}$ will be composed by fluctuation of u, v and C in each point of the domain. POD modes φ_k allow one to decompose the state vector as:

$$\mathbf{q}(\mathbf{x},\mathrm{t}) = \sum_{j=1}^{\infty} a_j(t)\boldsymbol{\varphi}_j(\mathbf{x}) \qquad (1)$$

where the coefficients $a_j(t)$ are the projections of the state vector over the modes. POD eigenvalues λ_k, represent how well each mode captures the original data in the L_2 norm sense, and one can truncate the series (1) to the order r such that $\sum_j^r \lambda_j / \sum_j^\infty \lambda_j \approx 1$.

1.3 SPOD technique

Following the works of Towne *et al.* [2] and of Schmidt *et al.* [3], the SPOD analysis allows one to extract the spectral features of the flow field. The snapshot ensemble can be divided in n_b blocks even overlapping and within each n^{th} block a windowed DFT is computed. Each Fourier component has now a realization for each block, and realizations can be stacked properly in matrix $\widehat{\mathbf{Q}}_{f_k}$ for each frequency f_k. A POD decomposition has to be performed on each matrix $\widehat{\mathbf{Q}}_{f_k}$, namely an eigenvalue/eigenvector problem for the cross-spectral correlation matrix $\boldsymbol{S}_{f_k} = \widehat{\mathbf{Q}}_{f_k}\widehat{\mathbf{Q}}_{f_k}^*$, to retrieve SPOD modes and eigenvalues for each frequency, namely $\boldsymbol{\Phi}_{f_k}$ and $\boldsymbol{\Lambda}_{f_k}$.

2 RESULTS

2.1 Supercritical regime

Panels (a) and (b) of Figure 2 report the normalized POD eigenvalues for the case *a* defined in Table 1, which refers to the dimensionless forcing frequency $\mathrm{St_a} = 0.076$ ($\mathrm{f_a} = 25\,Hz$) in supercritical regime $\mathrm{We} = 2.5$. It is interesting to notice that the first 2 modes contain about the 85% of the energy, while with only 10 modes the amount of energy rises up to about 99%.

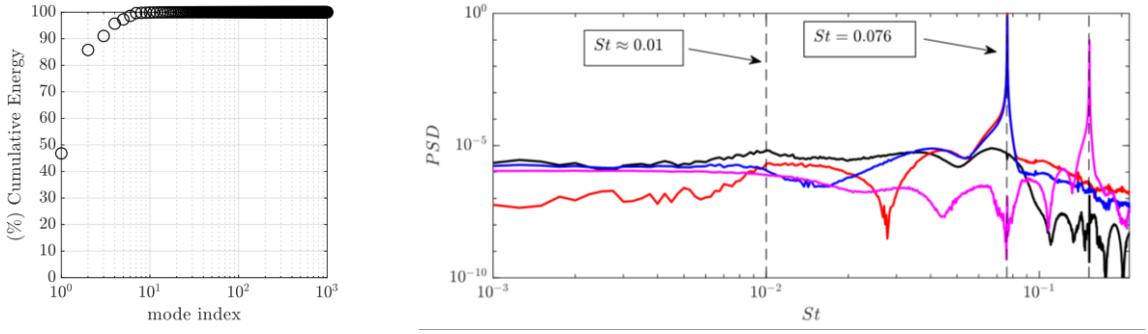

(a) (b)

Figure 2: (a): Energy content of POD modes for configuration *(a)* of Table 1. (b): Normalized PSD of embedded coordinates $a_j(t)$. Red line refers to the 1st mode, blue line to the 2nd mode, magenta line to the 3rd mode, and black line to 9th mode.

Power spectral density (PSD) of embedded coordinates $a_j(t)$ of selected modes, panel (b) of Figure 2, reveals that first and second modes present a very sharp peak at the actuation frequency capturing the most of the energy while at low frequencies the leading mode is the 9th even if its energy content is far less than the leading ones. This occurrence highlights one of the major limitations of POD technique. Moreover 9th mode has a peak at $\mathrm{St} \approx 0.01$ ($f \approx 3.5\,Hz$) which is the natural frequency of the linearized 1D inviscid model developed by Della Pia *et al.* [6]. The corresponding spatial distributions of the leading POD mode of pertubations of velocity, u' and v', and of the volume fraction, C', is reported in Figure 3 in which only sinuous motion can be recognized, namely an antisymmetric distribution of modes of u' and C' and a symmetric one for v'. The spatial structures of such modes correspond to the sketch depicting the sinuous disturbances reported in panel (d) of Figure 3.

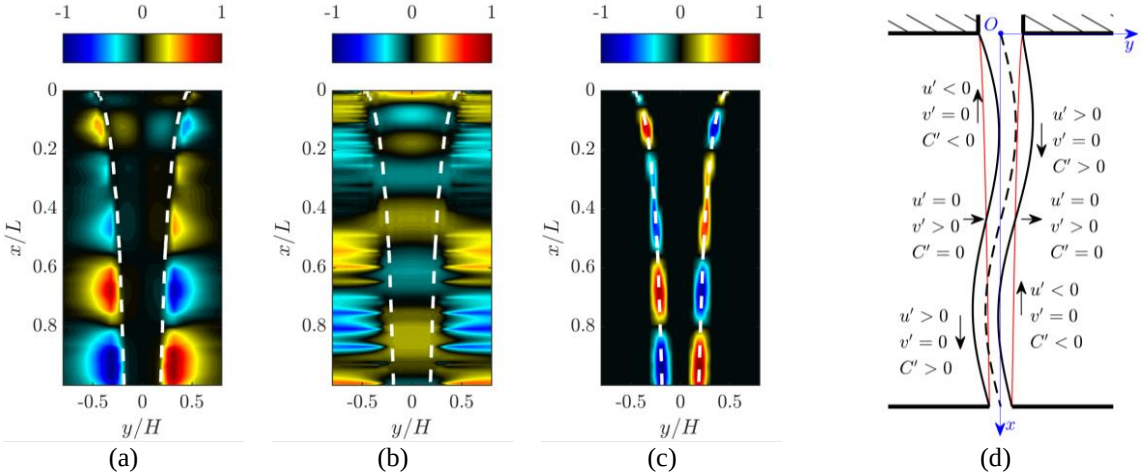

(a) (b) (c) (d)

Figure 3: (a): Leading POD mode of *u'*; (b): *v'*; (c): *C'*; (d): Sinuous perturbations sketch.

The application of SPOD technique sheds light into the system spectral behaviour, pointing out its characteristic frequencies. Here the SPOD analysis is carried out with a number of blocks $n_b = 12$ and a number of frequencies $n_f = 188$. The SPOD spectrum for the configuration *(a)* is shown in panel (a) of Figure 4. The flow presents the largest modal separation at the actuation frequency and its harmonics. Another separation region occurs at a lower frequency, $\mathrm{St} \approx 0.01$, that is associated, as

already argued in POD analysis, with the natural frequency of the 1D inviscid model. As shown in Della Pia *et al.* [6,7], supercritical regimes are characterized by natural oscillation frequencies which are one order of magnitude lower that the corresponding frequencies in subcritical conditions, as will be recovered by the modal analysis hereafter reported.

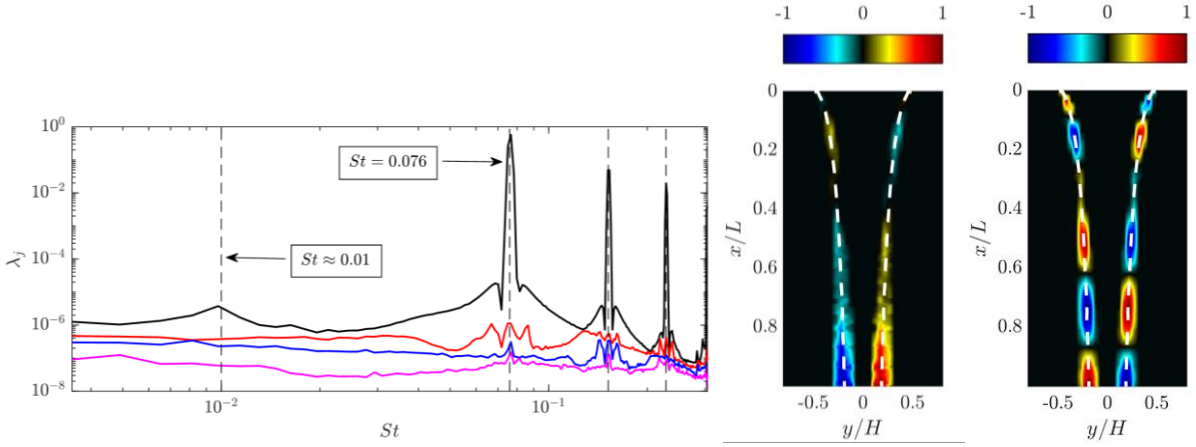

(a) (b) (c)

Figure 4: (a): SPOD spectrum for configuration *(a)* of Table 1. (b): Leading SPOD mode of C' at St ≈ 0.01. (c): Leading SPOD mode of C' at St = 0.076.

2.2 Subcritical regime

In subcritical regime some relevant features of the flow are carried out by means of modal analysis. Figure 5, panel (a), reports the PSD of selected embedded coordinates $a_j(t)$ for the configuration *(c)* of Table 1; it is straightforward to notice that at low frequencies no peak appear in the spectrum, while are obviously present peaks at forcing frequency and its harmonics. Panel (b) contains the cumulative energy distribution of POD modes for various Re numbers in subcritical regime. At high *Re* numbers performances of POD analysis degrade as at these flow regimes strong nonlinearities arise, and the linear POD technique is not a suitable tool to analyze these cases.

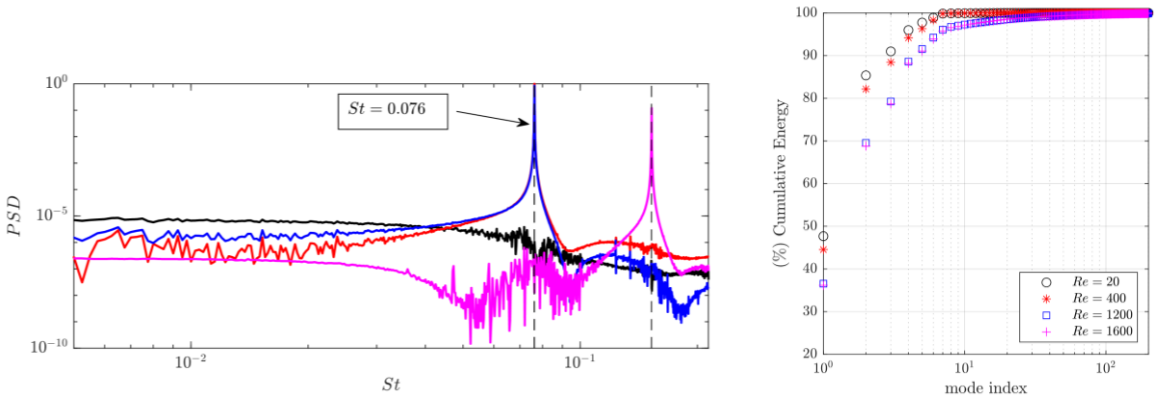

(a) (b)

Figure 5: (a): Normalized PSD of embedded coordinates $a_j(t)$. Red line refers to the 1st mode, blue line to the 2nd mode, magenta line to the 3rd mode, and black line to 8th mode. (b): Cumulative energy distribution of POD modes for various *Re* numbers in subcritical regime. Configurations from *(b)* to *(e)* of Table 1.

By means of SPOD analysis the emergence of a varicose deformation at high *Re*, even if the forcing is purely sinuous has been highlighted. Leading Fourier component of the 1st SPOD mode of configuration (e) of Table 1 is reported in panel (a) of Figure 6. Considering that each mode can be decomposed as: $\varphi_i = \varphi_i^v + \varphi_i^s$, where superscripts *v* and *s* stand for varicose and sinuous respectively, looking at panel (b) and (c), it is noticeable that a varicose deformation arises in this configuration. Panel (d) depicts a sketch of varicose perturbation.

In Figure 7 is reported a parametric SPOD analysis by varying the Reynolds number *Re* at *We* = 0.75 in panel (a) and by varying the Weber number *We* at *Re* = 1600 in panel (b). Panel (a) shows that

increasing *Re*, together with the appearance of varicose deformation, SPOD spectrum presents also peaks at subharmonics of the actuation, typical phenomenon of a nonlinear system.

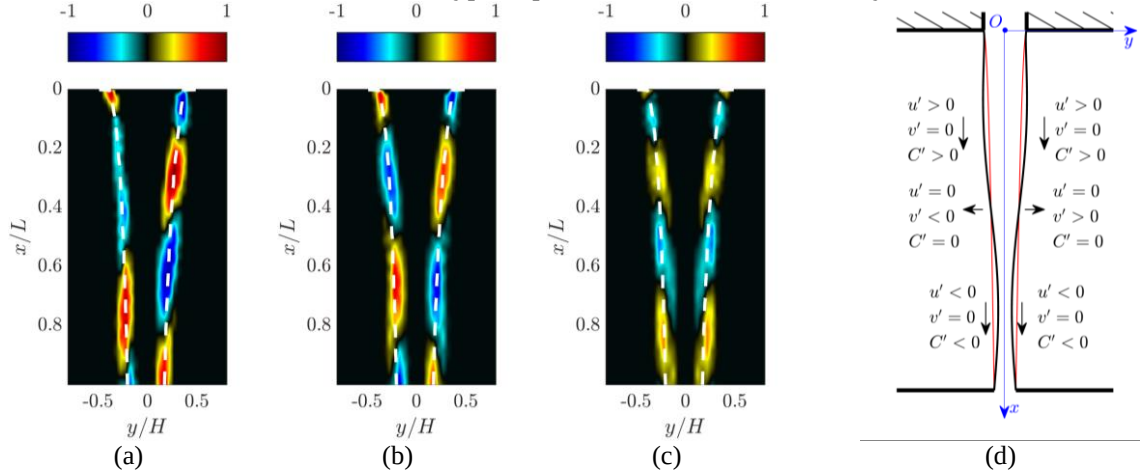

Figure 6: (a): Leading SPOD mode of *C'* at St = 0.076 for configuration *(e)* of Table 1. (b): Sinuous component. (c): Varicose component. (d): Varicose perturbation sketch.

In resonance conditions at high Reynolds number, namely by forcing at the natural frequency predicted by the 1D model, is subcritical regime, the flow exhibits also a varicose deformation. Panel (b) of Figure 7 shows how decreasing the *We* towards the values of 0.75 and 0.8, in concomitance of the superposition of sinuous and varicose deformation in the leading Fourier component of the 1st SPOD mode, peaks at subharmonics of the actuation frequency are detected.

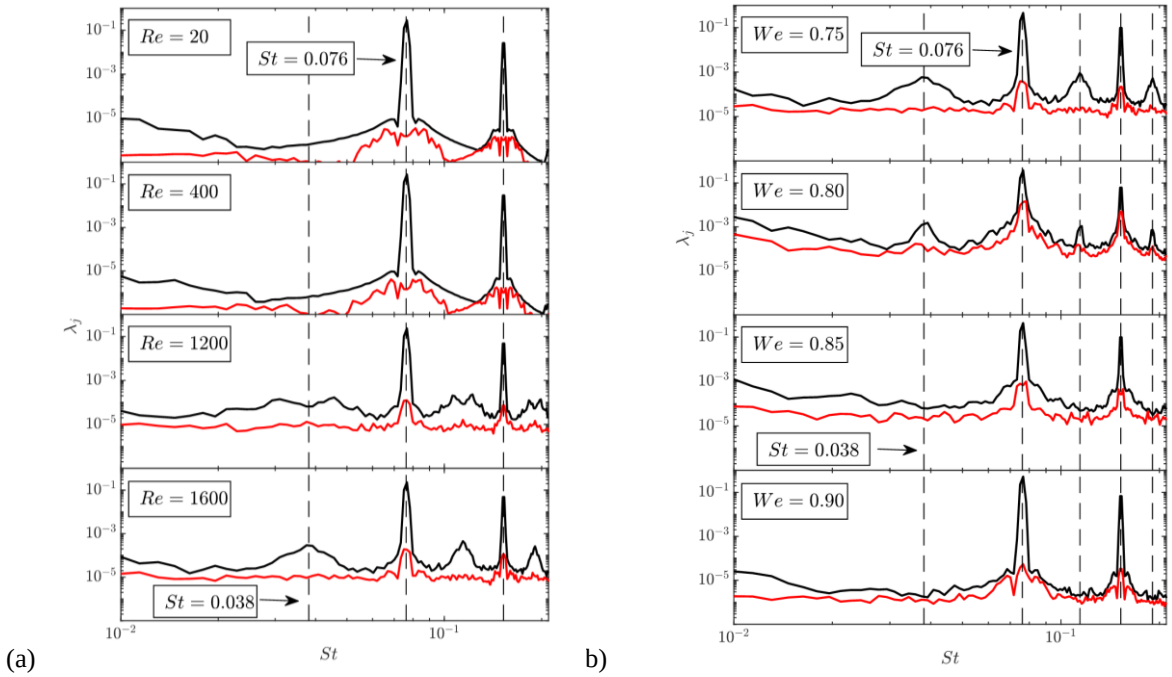

Figure 7: (a): SPOD spectra for configurations *(b)* to *(e)*. Effect of *Re*. (b): SPOD spectra for configurations *(e)* to *(i)*. Effect of *We*. The spectra report only the frequency content of the first 2 modes.

To highlight whether the flow presents the superposition of varicose and sinuous deformations, SPOD decomposition has been performed directly on the displacement of the meanline *l* and the thickness *h* of the liquid sheet, depicted in panel (a) Figure 1, for configurations *(e)* and *(h)* of Table 1. Panels from (a) to (c) of Figure 8 refer to *We* = 0.75 whilst panels from (d) to (e) refer to *We* = 0.85. Panels (b) and (c), that contain first 2 Fourier components of the 1st SPOD mode of configurations *(e)* (*We* = 0.75), show the superposition of varicose and sinuous modes whilst panels (e) and (f), referring to configuration *(h)* (*We* = 0.85) highlight a clear separation between them.

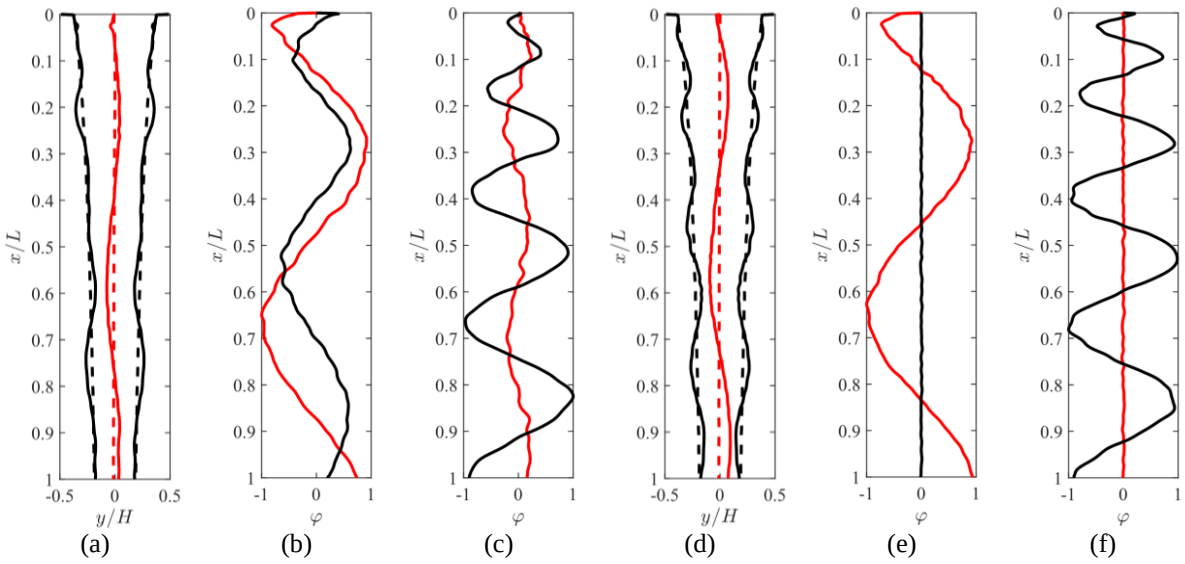

Figure 8: (a): Mean (dashed lines) and instantaneous (solid) of *h* (black) and *l* (red) of case (e) of Table 1. (b): 1st Fourier component of the 1st mode. (c): 2nd Fourier component of the 1st mode. (d): Mean and instantaneous of *h* and *l* of case (h). (e): 1st Fourier component of the 1st mode. (f): 2nd Fourier component of the 1st mode.

3 CONCLUSIONS

A modal analysis, including both POD and SPOD techniques, has been performed on two-dimensional two-phase numerical simulations data (obtained with the VOF code BASILISK) of vertical liquid sheets driven by a continuous harmonic perturbation in lateral velocity component applied at the inlet section, at several Reynolds numbers and Weber numbers.

In supercritical regime ($We > 1$) both POD and SPOD modes exhibit an analogous sinuous spatial structure, featuring a traveling perturbation. Both spectra confirm the occurrence of a discontinuity in frequency response between the supercritical and subcritical regimes. In subcritical regime ($We < 1$) the investigation highlighted the excitation of a combined sinuous-varicose motion when the system is forced at relatively high Reynolds number. The appearance of the varicose component is due to nonlinear coupling effects occurring in resonance conditions, i.e. when the sheet is driven by a frequency equal to that of leading natural frequency. Furthermore, it has been noticed that when the Weber number is decreased from We = 0.90 down to 0.75 the varicose perturbation shifts from the higher harmonics towards the main Fourier mode, and this can be considered as a prelude to the rupture of the liquid sheet when the flow rate is reduced. The latter hypothesis should be carefully verified by means of three-dimensional numerical simulations as well as experimental campaigns.

REFERENCES

[1] G. Berkooz, P. Holmes, and J. L. Lumley. “The proper orthogonal decomposition in the analysis of turbulent flows”. *Annual Review of Fluid Mechanics*, **25**, pp. 539-575 (1993).

[2] A. Towne, O. T. Schmidt, and T. Colonius. “Spectral proper orthogonal decomposition and its relationship to dynamic mode decomposition and resolvent analysis”. *Journal of Fluid Mechanics*, **847**, pp. 821-867 (2018).

[3] O. T. Schmidt and T. Colonius. “Guide to spectral proper orthogonal decomposition”. *AIAA Journal*, **58**, pp. 1023-1033 (2020).

[4] S. Popinet. “An accurate adaptive solver for surface-tension-driven interfacial flows”. *Journal of Computational Physics*, **228**, 5838-5866 (2009).

[5] R. Scardovelli and S. Zaleski. “Direct numerical simulation of free-surface and interfacial flow”. *Annual Review of Fluid Mechanics*, **31**, 567-603 (1999).

[6] A. Della Pia, M. Chiatto, and L. De Luca. “Global eigenmodes of thin liquid sheets by means of volume-of-fluid simulations”. *Physics of Fluids*, **32**, 082112 (2020).

[7] A. Della Pia, M. Chiatto, and L. De Luca. “Receptivity to forcing disturbances in subcritical liquid sheet flows”. *Physics of Fluids*, **33**, 032113 (2021).